Theoretical Investigation of the Neuronal Na^+ Channel *SCN1A*: Abnormal Gating and Epilepsy

Colleen E. Clancy and Robert S. Kass
Department of Pharmacology, Columbia University College of Physicians and Surgeons, New York, New York 10032

ABSTRACT Epilepsy is a paroxysmal neurological disorder resulting from abnormal cellular excitability and is a common cause of disability. Recently, some forms of idiopathic epilepsy have been causally related to genetic mutations in neuronal ion channels. To understand disease mechanisms, it is crucial to understand how a gene defect can disrupt channel gating, which in turn can affect complex cellular dynamic processes. We develop a theoretical Markovian model of the neuronal Na^+ channel $Na_V1.1$ to explore and explain gating mechanisms underlying cellular excitability and physiological and pathophysiological mechanisms of abnormal neuronal excitability in the context of epilepsy. Genetic epilepsy has been shown to result from both mutations that give rise to a gain of channel function and from those that reduce the Na^+ current. These data may suggest that abnormal excitation can result from both hyperexcitability and hypoexcitability, the mechanisms of which are presumably distinct, and as yet elusive. Revelation of the molecular origins will allow for translation into targeted pharmacological interventions that must be developed to treat syndromes resulting from divergent mechanisms. This work represents a first step in developing a comprehensive theoretical model to investigate the molecular mechanisms underlying runaway excitation that cause epilepsy.

INTRODUCTION

There has been renewed interest in the study of voltage-gated Na^+ channels since recent findings have implicated Na^+ channel mutations in clinical syndromes. The long QT syndrome has been linked to mutations in the cardiac channel gene *SCN5A* (Bennett et al., 1995), whereas hyperkalemic periodic paralysis, paramyotonia congenital, and potassium-aggravated myotonias may result from mutations in the skeletal muscle gene *SCN4A* (Hayward et al., 1996, 1997, 2001, 1999). Genetic abnormalities in the isoforms predominantly expressed in the CNS, including *SCN1A* (Escayg et al., 2001, 2000; Lossin et al., 2002, 2003; Meisler et al., 2002), *SCN2A* (Kearney et al., 2001), and *SCN8A* (Meisler et al., 2001, 1998) have been correlated with epilepsy, autism (Weiss et al., 2003), and abnormal neuronal excitation. Interestingly, all sodium channel-linked syndromes are characterized by episodic attacks and heterogeneous phenotypic manifestations (Goldin, 2001; Lerche et al., 2001a,b; Steinlein, 2001). Detailed understanding of the subtleties of normal and mutation-altered Na^+ channel gating will undoubtedly improve understanding of molecular mechanisms of disease phenotypes. Moreover, defective channels are potential targets for pharmacological interventions (Carmeliet et al., 2001; Goldin, 2001).

A common effect, albeit not exclusive (Clancy et al., 2003; Jurkat-Rott et al., 2000; Wehrens et al., 2000), of gene mutations across Na^+ channel subtypes is a propensity to disrupt inactivation (Alekov et al., 2001; Cossette et al., 2003; Hayward et al., 1999; Lossin et al., 2002). Normally wild-type (WT) Na^+ channels open in response to membrane depolarization, then enter absorbing inactivation states that prevent reopening during sustained depolarization (Catterall, 2000). Many Na^+ channel mutations linked to clinical syndromes exert their deleterious effects by disrupting the inactivation process either by reducing the rate of channel inactivation or by increasing the likelihood of recovery from inactivation (i.e., reducing the absorbency of inactivation) (Alekov et al., 2000; Balser, 1999; Bennett et al., 1995; Clancy and Rudy, 1999; Clancy et al., 2003; Hayward et al., 1999; Lossin et al., 2002).

To explicate the disease basis of ion channel-linked genetic disorders, it is crucial to understand how a gene defect can disrupt channel gating, which will affect complex interactive cellular dynamic processes. One approach to integration is through the use of transgenic animals. Another method is via the use of theoretical modeling techniques to build virtual transgenic cells (Noble, 2002b). Mathematical models are unique investigative tools in that they allow for high level integration of experimentally obtained data that is typically gathered in isolated expression systems, removed from the integrative cellular environment. As such, the relationship between the molecular findings and pathophysiology of the cell is difficult to discern.

As a first step toward computational integration, we develop a theoretical model of the brain Na^+ channel isoform $Na_V1.1$ encoded by *SCN1A*. Mutations in *SCN1A* have recently been linked to generalized epilepsy with febrile seizures plus (GEFS+) (Escayg et al., 2000; Lossin et al., 2002; MacDonald et al., 2001). $Na_V1.1$ is highly detectable in the cell bodies of the hippocampus, cerebellum, spinal cord, brainstem, cortex, substantia nigra, and caudate (Goldin, 2001). Recent studies also suggest $Na_V1.1$ as

Submitted November 25, 2003, and accepted for publication January 2, 2004.

Address reprint requests to Colleen E. Clancy, E-mail: cc2114@columbia.edu.

0006-3495/04/04/2606/09 $2.00

a primary player in normal synchronous coupling of ventricular depolarization and in control of heart rate in the sinoatrial node (Maier et al., 2002, 2003).

METHODS

Computational Methods

The Markov formulation of $Na_V1.1$ I_{Na} (Fig. 1) is an extension of the Clancy-Rudy model of the cardiac Na^+ channel (Clancy and Rudy, 1999, 2002) based on modeling efforts by Horn and Vandenberg (Horn and Vandenberg, 1984; Vandenberg and Horn, 1984).

Modeling macroscopic currents

Macroscopic current density is given by

$$I_s = G_s \times P_{O,s} \times (V_m - E_{rev}), \text{ where } G_s = s \times g_s.$$

$P_{O,s}$ is the sum of all channel open probabilities, V_m is the membrane potential, and E_{rev} is the reversal potential. G_s is the maximum membrane conductance density (channel density (σ) times the unitary channel conductance (g_s)).

The changes in channel-state probabilities are described by first-order differential equations. Assuming N discrete channel states, then the probability of the channel residing in a particular state P_i at any time satisfies

$$dP_i/dt = \sum_{j=1}^{N}[k_{ji} \times P_j(t, V_m)] - \sum_{j=1}^{N}[k_{ij} \times P_i(t, V_m)],$$

$$\text{for } i = 1, 2, \ldots, N-1;\ i \neq j \quad \text{and} \quad \sum_{i=1}^{N} P_i = 1.$$

The Nth state probability can be determined as the difference between 1 and the sum of the other $N-1$ state probabilities. The voltage- (V_m) dependent rate constants, k_{ij}, describe the transition from state i to state j. Initial conditions are obtained by finding values for state probabilities from the steady-state equation

$$dP_i/dt = 0.$$

Assuming that the probability in each state i at time t_n is

$$P_1(t_n),\ P_2(t_n),\ \ldots\ldots..P_N(t_n),$$

then at $t_{n+1} = t_n + dt$,

$$P_i(t_{n+1}) = P_i(t_n) + dP_i.$$

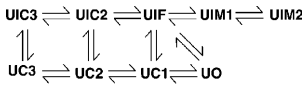

FIGURE 1 Markov model of the WT brain Na^+ channel isoform $Na_V1.1$. The model contains nine coupled states that represent channel activation, inactivation, and recovery from inactivation. See text for details.

dP_i is calculated at each time step. Picard iterates are computed by a second order Runge-Kutta procedure to obtain the dynamic values of P_i. The steady-state probability is used for $P_i(t_0)$ by allowing the simulated cell to rest until equilibrium is achieved (no change in computed parameters).

Single-channel gating

Stochastic properties of individual ion channels can be simulated as follows:

Given a simplified two-state model C $\leftrightarrow$ O, where at time = 0, the rate constant for the forward transition is *aa* and the rate for the reverse transition is *bb*, the channel resides in the C (closed) state, then the probability that the channel will transition to the O (open) state is determined by $e^{-(aa)T} = r$, where $T = ln(r)/-aa$, where r is a random number between 0 and 1. When time = T, then the channel will make a transition. The random number is generated by the computer function that is seeded by the internal clock, thereby ensuring that the sequence of random number generation is distinct each time. Microscopic reversibility was ensured by fixing the products of the forward and reverse transition rates in closed loops of the model.

All the simulations were encoded in C/C++ using Apple Developer Tools (Apple, Cupertino, CA). Simulations were implemented (double precision) on an Apple Macintosh dual 800MHz G4 processor running Apple OS X. Computer code used for computations in this article is available upon request by e-mailing cc2114@columbia.edu. Digitizelt software (ShareIt! Inc., Greensburg, PA) was used to extract experimental data from published plots.

RESULTS

Until recently Hodgkin-Huxley- (Hodgkin and Huxley, 1952) type models have been used as a modeling paradigm to represent currents in cellular action potential models (Beeler and Reuter, 1977; Traub et al., 1991; Migliore et al., 1995; Luo and Rudy, 1991, 1994). However, this framework is insufficient for incorporation of state-specific structural channel defects, in part because the Hodgkin-Huxley formalism presumes independence between kinetic transitions (Horn and Vandenberg, 1984; Vandenberg and Horn, 1984). Representation of coupling between discrete structural states is required to reproduce complex gating behaviors and especially to simulate mutations (Clancy and Rudy, 1999). Defects disrupting the structural integrity of a particular state will affect adjacent states.

We have formulated a Markovian-based model of $Na_V1.1$ that represents discrete structural states and their interactions. We develop the model based upon, and validated by comparison to, recent experimental data obtained in mammalian expression systems. We then introduce an experimentally characterized genetic defect, substitution of arginine by histidine at position 1648 (Escayg et al., 2000; Lossin et al., 2002; Spampanato et al., 2001), in *SCN1A* that has been causally linked to familial epilepsy as an example of the usefulness of the model. The mutation is located in the highly conserved positively charged voltage sensor in the fourth transmembrane segment of the fourth domain (Escayg et al., 2000; Spampanato et al., 2001). We investigate the gating of WT and R1648H mutant channel gating at the level of the cell and propose mechanisms of abnormal single-channel gating that explain the experimental observations.

Finally, we impose the waveform of a neuronal action potential to examine the mutant Na^+ channel current under conditions of changing voltage that mimic the physiological actuality. In doing so, we gain insight into possible means of abnormal cellular excitability that may trigger epileptiform activity, as well as elucidate mechanisms of normal and anomalous neuronal Na^+ channel gating.

The Markov model of *SCN1A* I_{Na} is shown in Fig. 1. The model representation corresponds to the ''normal mode'', which is sufficient to accurately simulate experimentally kinetic properties of normal or WT Nav1.1 channels. The model has nine discrete states consisting of three closed states (UC3, UC2, and UC1), a conducting open state (UO), a fast inactivation state (UIF), and two intermediate inactivation states (UIM1 and UIM2), the latter three of which are required to reproduce the complex fast and slow features of recovery from inactivation. Channel closed-state inactivation is achieved via the inclusion of two closed-inactivation states (UIC2 and UIC3). In response to depolarization, channels open and then rapidly inactivate after which they enter slower, more absorbing inactivation states. Each transition through a discrete state represents a putative conformational change at the level of the single-channel protein. In this way we have tried to relate the model to possible transitions that channels undergo in response to changing membrane potential. Channel movement through the UC states (i.e., UC3 → UC2 → UC1) represents individual movement of positively charged voltage sensors located in the fourth transmembrane segment of each of four channel domains. Fast inactivation (UO → UIF) corresponds to interaction of the intracellular linker between α-subunit domains III and IV with DIVS6 (McPhee et al., 1995). Slower inactivation (i.e., UIF → UIM1 → UIM2) represents more absorbing channel inactivation that follows fast inactivation.

Fig. 2 *A* compares experimentally recorded (*solid squares*) (Lossin et al., 2002) and simulated (*open circles*) activation and steady-state availability. Activation curves are constructed by normalizing the peak I_{Na} after depolarization from −120 mV to indicated depolarizing test potentials to the largest peak $Na_V1.1$ I_{Na}. Availability curves reflect the relative reduction of peak current plotted as a function of peak current at −20 mV after a long (sufficient to allow for steady state where the derivatives of the simulated channel-state probabilities are zero) prepulse to the test potential. Recovery from inactivation in experiments (Fig. 2 *B*, *solid squares*) (Lossin et al., 2002) and simulation (Fig. 2 *B*, *open circles*) are also shown. The ratio of peak current during the second pulse to peak current during the initial pulse is shown for WT channels. The logarithmic scale (*inset*) clearly illustrates the multi-exponential process of channel recovery from inactivation, an indicator of multiple inactivation states and recovery processes. The recovery from inactivation process is complex and highly coupled. The curve represents transitions out of all of the inactivation states (UIM2, UIM1, UIF, UIC2, and UIC3) and is well represented with the Markov scheme.

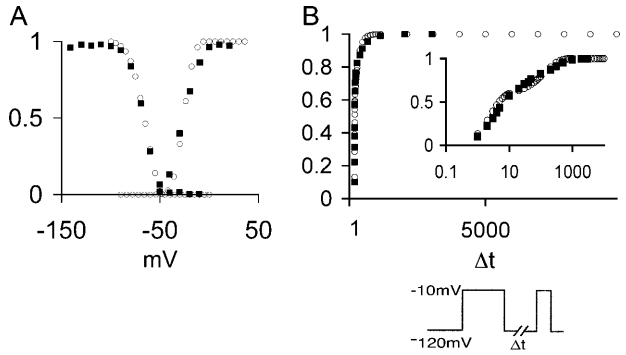

FIGURE 2 Experimentally recorded (Lossin et al., 2002) and simulated $Na_V1.1$ channel kinetics. (*A*) Experimentally recorded (Lossin et al., 2002; *solid squares*) and simulated (*open circles*) $Na_V1.1$ activation and inactivation. Activation $V_{1/2\ m}$ = (−26.4 mV), availability $V_{1/2\ h}$ = (−67.5 mV). (*B*) Recovery from inactivation in experiments (Lossin et al., 2002; *solid squares*) and simulations (*open circles*). Inset is an expanded log timescale. Peak I_{Na} elicited by the second pulse after the variable recovery period is normalized to peak I_{Na} during first pulse. Protocol is shown as inset under *B*.

The slow components of channel recovery from inactivation in $Na_V1.1$ result in a rate-dependent reduction in peak current during a pacing protocol. Fig. 3 illustrates the rate-dependent reduction in peak current (normalized to the maximum current measured on the first beat) in experimental recordings from a hippocampal CA1 pyramidal neuron dendritic cell-attached patch (Fig. 3 *A*) (Colbert and Johnston, 1998) and simulations (Fig. 3 *B*). It should be noted that although Nav1.1 has been shown to localize within the soma and dendrites of neurons in the hippocampus (Westenbroek et al., 1989), Colbert and Johnston did not show specifically that the recorded current was from $Na_V1.1$. Nonetheless, the pace-dependent reduction in macroscopic Na^+ current illustrates the importance of slow channel recovery from inactivation in determining cellular neuronal excitability. Cells were subjected to 10 paced beats to −5 mV for 2 ms followed by 100 ms repolarization to −65 mV. Notably, after 10 paced beats, the peak current is reduced by >50%. This reduction occurs due to a buildup of channel inactivation and an insufficient recovery period between beats to allow for channel recovery from inactivation. Interestingly, the degree of current reduction is much greater than observed with the cardiac isoform (Clancy et al., 2002), consistent with markedly slower channel recovery from inactivation (Fig. 2 *B*) observed in $Na_V1.1$.

Thus far, we have demonstrated that the Markovian model of WT *SCN1A* I_{Na} can recapitulate the major kinetic gating features observed experimentally, including the voltage dependence of availability and activation, as well as the time dependence of channel recovery from inactivation. The model can also account for the pulse-dependent reduction in peak current, which reflects complex interactions, including

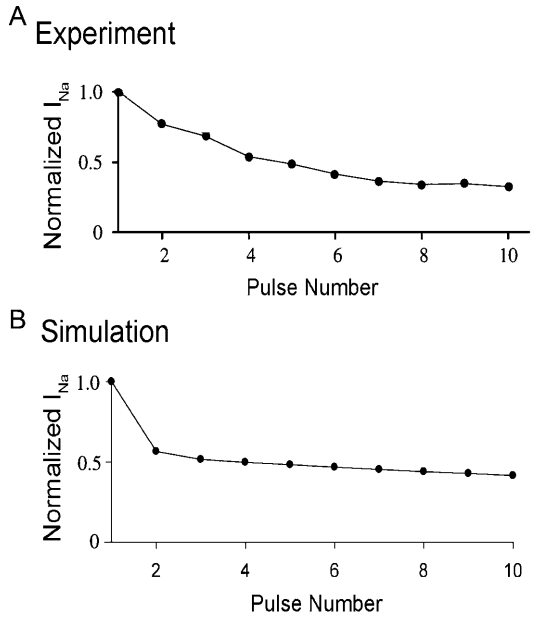

FIGURE 3 Rate-dependent reduction of peak I_{Na}. Experimentally (Colbert and Johnston, 1998) recorded Na^+ current from CA1 hippocampal dendrites (*A*) and simulated (*B*) $Na_V1.1$ peak I_{Na} is reduced with repetitive pulsing. Depolarization to −5 mV for 2 ms with 100 ms recovery interval to the holding potential (−65 mV) results in a buildup of channel inactivation and resulting rate-dependent reduction of peak I_{Na}. In both the experiment (Colbert and Johnston, 1998) and simulation, the 10th pulse elicits <50% of peak I_{Na} measured during the first pulse.

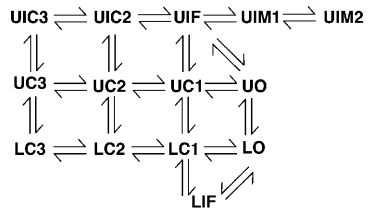

FIGURE 4 Markov model of the brain Na^+ channel isoform $Na_V1.1$. The channel model contains normal (*upper nine states*) and flicker (*lower five states*) gating modes. The vast majority of channels reside in the normal mode, but mutations increase the probability of entry into the abnormal gating mode. The flicker mode is identical to the normal mode except that it lacks stable inactivation states. The mode reflects a population of channels that transiently inactivate and then rapidly recover and reopen.

the time and voltage-dependent activation, open-state inactivation, and recovery processes. We next investigated the feasibility of utilizing the model to simulate mutation-induced changes in channel gating.

A ''modal gating'' scheme, which represents a subpopulation of channels that is computed as a probability of entry into the alternate mode, can be used to account for all of the observed macroscopic current properties and is shown in Fig. 4. Experiments suggest that the R1648H mutation dramatically increases the channel open probability in a subpopulation of channels (Lossin et al., 2002; Vanoye et al., 2003) with relatively short open times (Vanoye et al., 2003). This anomalous gating behavior can be feasibly modeled as a ''flicker'' mode of gating. This gating mode is identical to the normal mode, except that stable inactivation is disrupted. Hence, the stable inactivation states present in the normal mode are absent (i.e., UIC3, UIC2, UIM1, and UIM2). In the flicker mode (lower five states, prefixed with ''L''), channels enter the fast inactivation state, but do not slow inactivate. This allows for channels to recover from fast inactivation and reopen (LIF → LC1 → LO). Transition rates between upper and lower states represent a probability of transition between the two modes of gating. In other words, channels in the flicker mode correspond to a subpopulation of channels that open and fast inactivate exactly like channels in the normal mode, but then they fail to enter more stable absorbing inactivation states. Although the modal gating scheme that we implement appears complicated (14 states), from a structural perspective it actually represents the disruption of stable inactivation in a small subpopulation of channels. It is notable that flickering channels have shorter open times compared to bursting channels (Clancy et al., 2002). This is due to the fact that the open time is determined by the inactivation transition in flickering channels, and the slower deactivation transition in bursting channels.

Fig. 5 illustrates single-channel gating of WT and R1648H mutant channels in the normal mode (upper states prefixed by ''U'' in model scheme in Fig. 4) predicted by the model. WT channels in the normal mode open and inactivate in response to depolarization. Although there are infrequent reopenings during sustained depolarization, most channels open once in response to the onset of depolarization and then inactivate. These infrequent (low probability) reopenings account for the small persistent late current component (0.3% of peak) observed in WT cells.

In contrast, channels in the flicker mode are shown with the corresponding Markov representation (Fig. 5, *left panels*). Flickering channels inactivate after opening (LO → LIF), but fail to enter slower, more stable inactivation states (absence of UIM1 and UIM2 as in normal mode in Fig. 4). As a result, channels frequently reopen and reinactivate.

WT and R1648H $Na_V1.1$ macroscopic current are shown in Fig. 6 (*top*, experiments (Lossin et al., 2002) and *bottom* simulations). In the WT channels, depolarization to −20 mV from a holding potential of −140 mV (where all channels are available to open) results in a large macroscopic current (peak >300 A/F) that fully inactivates and nearly decays to the zero current level (0.3% of the peak). In contrast, a model cell with a R1648H mutant channel population is marked by a persistent component (4.2% of peak) of current even after prolonged depolarization (200 ms). This aberration in the macroscopic mutant current phenotype indicates that the R1648H mutation disrupts channel inactivation that occurs subsequent to channel opening. The larger persistent current is the primary effect of the mutation on the macroscopic

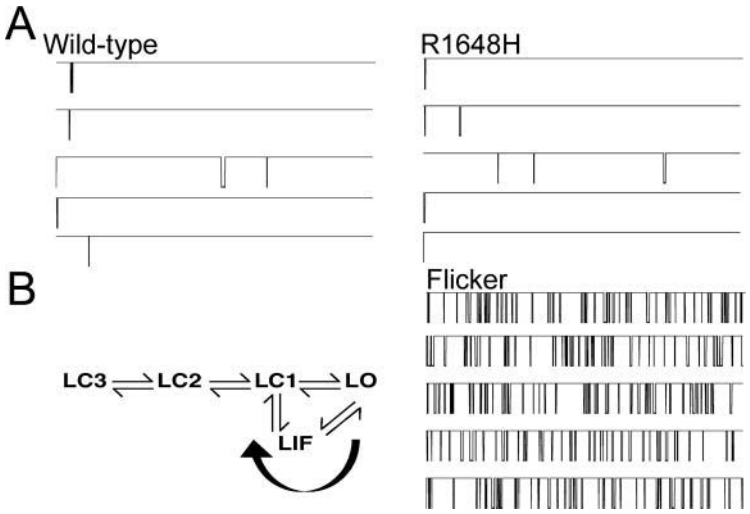

FIGURE 5 Simulated stochastic single-channel gating of WT and R1648H $Na_V1.1$ I_{Na}. Channel opening is denoted by downward deflections. (*A*) Five consecutive WT (*left*) and R1648H (*right*) mutant channel gating in the normal mode (*upper nine states*) elicited by depolarization to 0 mV from a holding potential of −120 mV. (*B*) Single-channel gating is shown in the abnormal flicker mode, whereby channels open and fast inactivate, but then recover from inactivation and reopen.

current, as there is no significant change in the voltage dependence of channel activation, availability, or recovery from inactivation (Table 1 (Lossin et al., 2002)) measured during the protocols used in Fig. 2.

The voltage dependence of the mutation-altered late current can be measured directly by using a slow positive ramp pulse protocol. In keeping with experiments by Lossin et al. (2002), we used a positive ramp protocol (slow voltage ramp from −120 mV to +40 mV in 8 s) to investigate the $Na_V1.1$ R1648H ramp current (Fig. 7). The ramp current morphology is comparable between experimentally (Lossin et al., 2002) recorded R1648H I_{Na} (Fig. 7, *top*) and simulation (*bottom*). Interestingly, the voltage dependence of the late current is nearly identical to the macroscopic current voltage relationship. This suggests that the amplitude of the mutant late current is primarily determined by the driving force ($V_m - V_r$) for Na^+. These data imply that the voltage-dependent gating process of activation is the same for both macroscopic peak and late current and that the late current results from a limited population of channels that activate normally and then subsequently fail to properly inactivate. It is also noteworthy that the representation of mutant channel gating by flicker modal gating can account for the voltage independence of the ramp current shown in Fig. 7.

Thus far, we have established the capability of the Markov Na^+ channel model to correctly reproduce macroscopic current properties of WT and R1648H mutant $Na_V1.1$ channels. We also suggest flicker modal single-channel gating that can account for the whole cell properties. To attempt to gain insights into the potential mechanism of disruption of cellular activity by the R1648H mutation, we developed a neuronal action potential (AP) clamp protocol to allow observation of the WT and mutant channel currents under conditions of changing voltage that mimic the physiological membrane potential.

Fig. 8 illustrates the imposition of an AP waveform voltage clamp protocol for WT (*A*) and R1648H (*B*) cases, and the corresponding I_{Na} shown beneath each voltage clamp. The 10th–12th pulses are shown. From steady state at a holding potential of −65 mV, simulated cells were gradually depolarized (50 ms interval) to −55 mV and then rapidly depolarized 20 mV, followed by 10 ms repolarization (representing neuronal AP duration (Traub et al., 1991)) to −65 mV. The R1648H mutant I_{Na} (Fig. 8 *B*, *lower panel*) has a larger peak current (explanation below) and a dramatically increased persistent current (*arrow*) compared to WT. Notably, the amplitude of the persistent current during the repolarizing ramp is more than half the amplitude of the peak current elicited by the depolarization to 20 mV. This seems unlikely, since the currents in Fig. 6 display a persistent current component that is only 4.2% of peak in the mutant case. However, although the fraction of channels residing in the abnormal flicker and/or burst mode is very small, the physiological holding potential of −65 mV results in a majority of channels residing in inactivation states (as would be predicted by the availability curve in Fig. 2). Hence, channels in an abnormal gating mode that exhibit anomalous inactivation result in a component of current that is significant at physiological membrane potentials. An interesting finding is that channels in the abnormal gating mode also contribute to the peak I_{Na} in response to the fast mimicked AP upstroke, resulting in a larger transient I_{Na} in the R1648H case compared to WT. The larger peak current in the R1648H mutant was not predicted by the voltage protocol in Fig. 6, where the holding potential of −140 mV results in all of the channels being available to open in response to depolarization. In that case, the late current is relatively small compared to peak and does not significantly contribute to the peak transient current. However, the late current (i.e., probability of residence in the abnormal gating mode) is relatively voltage independent (Fig. 7) and the

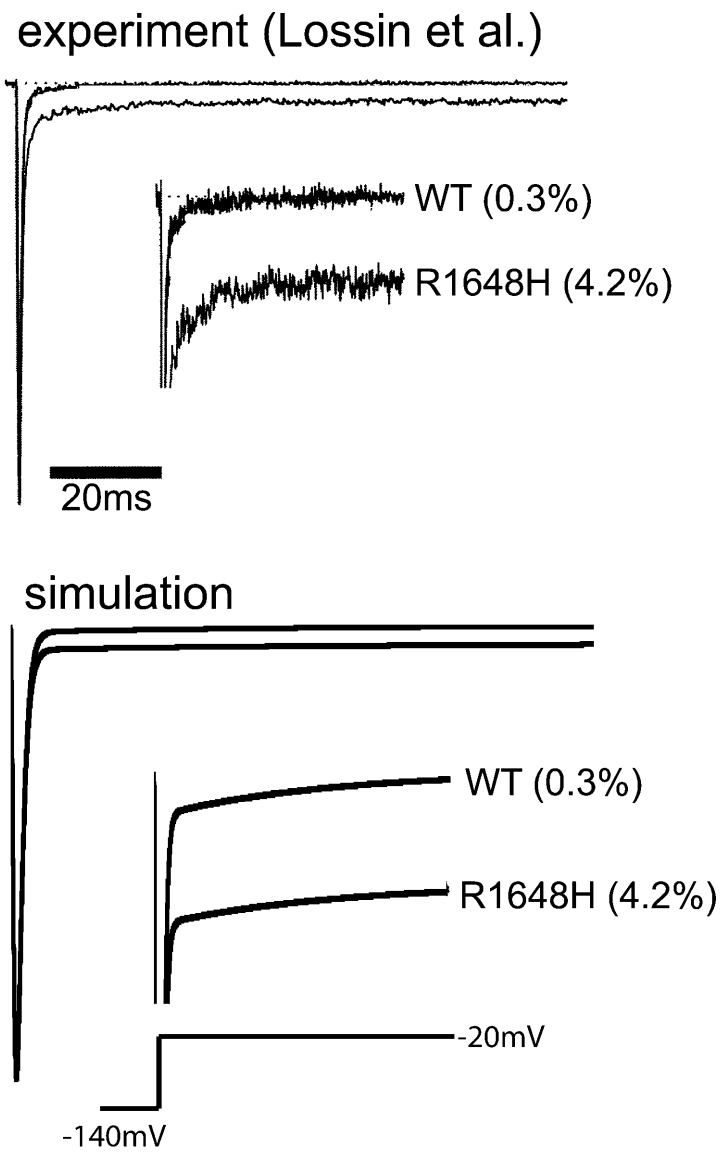

FIGURE 6 The R1648H mutation in $Na_V1.1$ is linked to epilepsy and causes abnormal inactivation resulting in persistent current. Experimental (Lossin et al., 2002) WT and R1648H mutant whole cell current shown in (*top*) at low and high *(inset)* gain. Simulated currents of the R1648H mutant are shown in bottom panel.

contribution to the upstroke that occurs after depolarization from the physiological rest potential in Fig. 8 (−65 mV) is much larger. This occurs due to the fact that the relative probability in the abnormal versus the normal mode is significant, resulting in a sufficiently large fractional contribution of the flickering channels to increase the transient current during the upstroke.

TABLE 1

	Wild-type $Na_V1.1$	R1648H mutant $Na_V1.1$
Activation $V_{1/2}$	−26.4 mV*	−25.9 mV*
Availability $V_{1/2}$	−67.5 mV*	−69.1 mV*
Recovery from inactivation	(τ_f = 6.4 ms, τ_s = 263 ms)*	(τ_f = 3.1 ms, τ_s = 257 ms)*

R1648H does not affect the kinetics of activation, availability or recovery from inactivation compared to WT in experiments (Lossin et al., 2002). Hence, these model parameters are unchanged in the mutant model scheme.
*n.s. versus WT.

DISCUSSION

Theoretical models are tools that allow exploration into complex protein behavior and ultimately cellular outcomes related to disruption of delicately balanced physiological processes (Noble, 2002a,b). Moreover, models can be extraordinarily useful to guide experimentation and may even suggest novel approaches (Clancy et al., 2003). We develop a Markovian computational model of the neuronal Na^+ channel $Na_V1.1$ encoded by *SCN1A* as a first step toward integration of genetic defects in integrative transgenic cellular models of hippocampal neurons. We demonstrate the potential for the model to simulate gating processes observed experimentally (Lossin et al., 2002; Vanoye et al.,

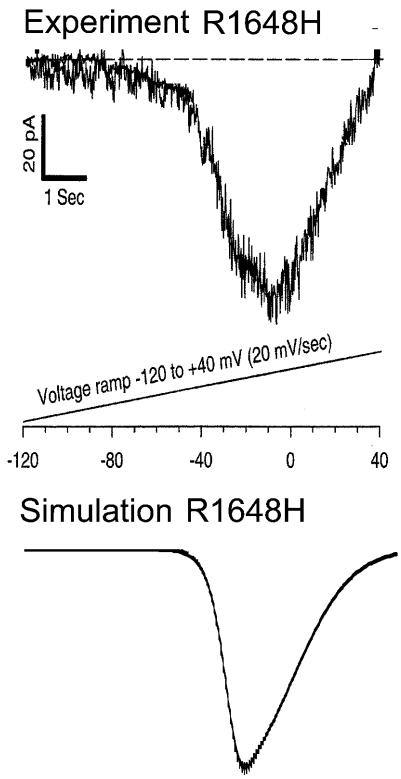

FIGURE 7 Experimentally recorded (Lossin et al., 2002) and simulated mutant R1648H $Na_V1.1$ I_{Na} during a positive ramp protocol. ''Window'' noninactivating current was measured using a slow ramp protocol (from −120 mV to +40 mV in 8 s). In experiment and simulation, the peak transient I_{Na} was increased threefold by the mutation.

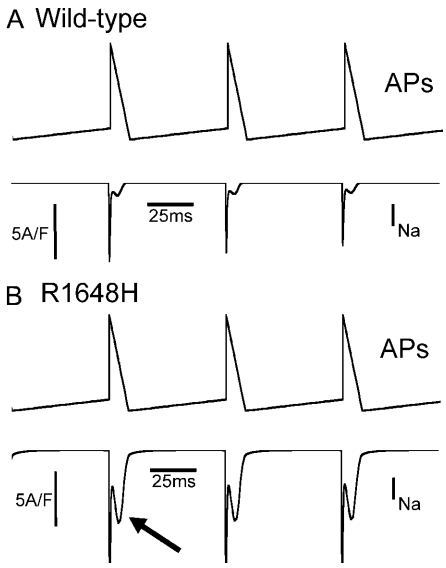

FIGURE 8 Simulated mutant R1648H $Na_V1.1$ I_{Na} during a simulated action potential clamp protocol that approximates a neuronal action potential. The negative ramp is from +20 mV to −60 mV for 10 ms with 50 ms interpulse intervals (cycle length = 60 ms). Panel *A* (*top*) illustrates the 10th–12th mimicked neuronal action potentials containing WT $Na_V1.1$ (*bottom*). The same protocol is shown in panel *B* (*top*) with corresponding R1648H I_{Na} (*bottom*). The R1648H mutation results in larger late I_{Na} compared to WT (*arrow*).

2003) and propose a modal single-channel gating scheme that accounts for the experimental data. Finally we investigate the morphology of the normal and mutant I_{Na} under conditions of changing voltage that mimic the physiological membrane potential during an action potential.

There are two primary effects of the R1648H mutation on $Na_V1.1$ I_{Na}. The first is an increase in the peak current. A fraction of channels that have impaired inactivation contribute to the action potential upstroke, which will act to result in an increase in the activation velocity and affect the peak upstroke voltage. The overall consequence is hyperexcitability, which may result in a tissue level predilection for runaway excitation. Slight increases in peak current have been shown previously to result in a predisposition to drug-induced arrhythmias in cardiac simulations (Splawski et al., 2002). The second effect of R1648H-induced alterations in channel inactivation will have consequences during repolarization.

An interesting question is how the R1648H mutation, which is located in the highly conserved positively charged voltage sensor in the fourth transmembrane segment of the fourth domain (Escayg et al., 2000; Spampanato et al., 2001), results in a disruption of inactivation, but no obvious alteration in activation gating. One might speculate that the effect of the mutation on the voltage dependence of activation is masked by the three normal voltage sensing S4 segments in domains I, II, and III. The intracellular side of the sixth transmembrane spanning segment of domain IV is the putative interaction (i.e., docking) site of the inactivation gate comprised of the intracellular linker between domains III and IV (McPhee et al., 1995). The effect on inactivation could conceivably result from an allosteric effect of the mutation on this docking site.

Although the neuronal action potential lacks the plateau phase that is critical in cardiac cells, the R1648H mutation may disrupt repolarization of the neuronal AP by altering the duration or morphology of the action potential. A secondary influx of Na^+ could potentially drive a spike after depolarization or lead to a burst of action potentials (Traub et al., 1994; Azouz et al., 1996; Brumberg et al., 2000). An analogy may perhaps be drawn between the morphology of the neuronal action potential and the murine cardiac action potential, which due to the rapidity of the mouse heart rate also lacks a well-defined plateau phase. Nonetheless, transgenic mice that carry the ΔKPQ mutation (Nuyens et al., 2001), a deletion mutation in the cardiac III-IV linker known to be a structure required for channel inactivation, exhibit AP plateaus and abnormally prolonged repolarization phases.

The interpretation described above is also consistent with epilepsy and other seizure disorders that are linked to genetic mutations in neuronal potassium channels, in particular those in the KCNQ family (Jentsch, 2000). Loss of K^+ channel

function would be expected to reduce the rate of repolarization and affect the duration of the action potential. Reduction of GABA-ergic inhibition resulting from defects in $GABA_A$ receptors is also consistent with the promotion of hyperexcitability (Baulac, 2001).

Another mechanistic possibility is that an increase in the neuronal membrane conductance to Na^+ throughout the action potential may result in secondary effects on the chemical and electrical driving force for other ionic currents, which are important in the context of homeostasis in the extracellular space (Jentsch, 2000). An increase in Na^+ conductance may sufficiently alter the membrane potential and increase the driving force (and membrane conductance) to K^+ or reduce the Ca^{2+} conductance. These alterations may occur heterogeneously along the neuron where a diversity of ionic conductance is observed (Traub et al., 1991). It is difficult to assess at this juncture whether these secondary manifestations might result in hyper- or hypoexcitability.

It must be noted, however, that modeling of complex biological processes is not without limitations. By definition, a model is a simplification of the actual biological process, which allows for insight and understanding, but may result in the exclusion of details necessary for absolute understanding of biological complexity and mechanism (Noble, 2002a,b). Nonetheless, the combination of theoretical prediction and experimental verification may lead to the identification of mechanisms by which genetic defects can underlie the development of clinical syndromes.

This work was supported by grants 1R01-HL 56810-5 and 1P01-HL 67849-02 from the United States Public Health Service to R.S.K. This work was also supported by The Epilepsy Foundation.

REFERENCES

Alekov, A. K., M. M. Rahman, N. Mitrovic, F. Lehmann-Horn, and H. Lerche. 2000. A sodium channel mutation causing epilepsy in man exhibits subtle defects in fast inactivation and activation in vitro. *J. Physiol.* 529:533–539.

Alekov, A. K., M. Rahman, N. Mitrovic, F. Lehmann-Horn, and H. Lerche. 2001. Enhanced inactivation and acceleration of activation of the sodium channel associated with epilepsy in man. *Eur. J. Neurosci.* 13:2171–2176.

Azouz, R., M. S. Jensen, and Y. Yaari. 1996. Ionic basis of spike after-depolarization and burst generation in adult rat hippocampal CA1 pyramidal cells. *J. Physiol.-London.* 492:211–223.

Balser, J. R. 1999. Sodium ''channelopathies'' and sudden death: must you be so sensitive? *Circ. Res.* 85:872–874.

Baulac, S., G. Huberfeld, I. Gourfinkel-An, G. Mitropoulou, A. Beranger, J. F. Prud'homme, M. Baulac, A. Brice, R. Bruzzone, and E. LeGuern. 2001. First genetic evidence of GABA(A) receptor dysfunction in epilepsy: a mutation in the gamma 2-subunit gene. *Nat. Genet.* 28:46–48.

Beeler, G. W., and H. Reuter. 1977. Reconstruction of the action potential of ventricular myocardial fibers. *J. Physiol.* 268:177–210.

Bennett, P. B., K. Yazawa, N. Makita, and A. L. George, Jr. 1995. Molecular mechanism for an inherited cardiac arrhythmia. *Nature.* 376:683–685.

Brumberg, J. C., L. G. Nowak, and D. A. McCormick. 2000. Ionic mechanisms underlying repetitive high-frequency burst firing in supragranular cortical neurons. *J. Neurosci.* 20:4829–4843.

Carmeliet, E., H. A. Fozzard, M. Hiraoka, M. J. Janse, S. Ogawa, D. M. Roden, M. R. Rosen, Y. Rudy, P. J. Schwartz, and P. S. Matteo. 2001. New approaches to antiarrhythmic therapy, Part I: emerging therapeutic applications of the cell biology of cardiac arrhythmias. *Circulation.* 104:2865–2873.

Catterall, W. A. 2000. From ionic currents to molecular mechanisms: the structure and function of voltage-gated sodium channels. *Neuron.* 26: 13–25.

Clancy, C. E., and Y. Rudy. 1999. Linking a genetic defect to its cellular phenotype in a cardiac arrhythmia. *Nature.* 400:566–569.

Clancy, C. E., and Y. Rudy. 2002. Na^+ channel mutation that causes both Brugada and long-QT syndrome phenotypes: a simulation study of mechanism. *Circulation.* 105:1208–1213.

Clancy, C. E., M. Tateyama, and R. S. Kass. 2002. Insights into the molecular mechanisms of bradycardia-triggered arrhythmias in long QT-3 syndrome. *J. Clin. Invest.* 110:1251–1262.

Clancy, C. E., M. Tateyama, H. Liu, X. H. T. Wehrens, and R. S. Kass. 2003. Non-equilibrium gating in cardiac Na^+ channels: an original mechanism of arrhythmia. *Circulation.* 107:2233–2237.

Colbert, C. M., and D. Johnston. 1998. Protein kinase C activation decreases activity-dependent attenuation of dendritic Na^+ current in hippocampal CA1 pyramidal neurons. *J. Neurophysiol.* 79:491–495.

Cossette, P., A. Loukas, R. G. Lafreniere, D. Rochefort, E. Harvey-Girard, D. S. Ragsdale, R. J. Dunn, and G. A. Rouleau. 2003. Functional characterization of the D188V mutation in neuronal voltage-gated sodium channel causing generalized epilepsy with febrile seizures plus (GEFS). *Epilepsy Res.* 53:107–117.

Escayg, A., A. Heils, B. T. MacDonald, K. Haug, T. Sander, and M. H. Meisler. 2001. A novel SCN1A mutation associated with generalized epilepsy with febrile seizures plus—and prevalence of variants in patients with epilepsy. *Am. J. Hum. Genet.* 68:866–873.

Escayg, A., B. T. MacDonald, M. H. Meisler, S. Baulac, G. Huberfeld, I. An-Gourfinkel, A. Brice, E. LeGuern, B. Moulard, D. Chaigne, C. Buresi, and A. Malafosse. 2000. Mutations of SCN1A, encoding a neuronal sodium channel, in two families with GEFS+2. *Nat. Genet.* 24:343–345.

Goldin, A. L. 2001. Resurgence of sodium channel research. *Annu. Rev. Physiol.* 63:871–894.

Hayward, L. J., R. H. Brown, and S. C. Cannon. 1996. Inactivation defects caused by myotonia-associated mutations in the sodium channel III-IV linker. *J. Gen. Physiol.* 107:559–576.

Hayward, L. J., R. H. Brown, and S. C. Cannon. 1997. Slow inactivation differs among mutant Na channels associated with myotonia and periodic paralysis. *Biophys. J.* 72:1204–1219.

Hayward, L. J., J. S. Kim, G. Jang, F. F. Wu, C. Asada, V. Reid, D. P. Cros, E. P. Hoffman, S. C. Cannon, and R. H. Brown. 2001. A Na channel mutation associated with hyperkalemic periodic paralysis causes myotonia, K-induced weakness, and myopathy in mouse skeletal muscle. *Neurology.* 56:A81–A81. (Abstr.)

Hayward, L. J., G. M. Sandoval, and S. C. Cannon. 1999. Defective slow inactivation of sodium channels contributes to familial periodic paralysis. *Neurology.* 52:1447–1453.

Hodgkin, A. L., and A. F. Huxley. 1952. A quantitative description of membrane current and its application to conduction and excitation in nerve. *J. Physiol.* 117:500–544.

Horn, R., and C. A. Vandenberg. 1984. Statistical properties of single sodium-channels. *J. Gen. Physiol.* 84:505–534.

Jentsch, T. 2000. Neuronal KCNQ potassium channels: physiology and role in disease. Nat Rev Neurosci. 1:21–30.

Jurkat-Rott, K., N. Mitrovic, C. Hang, A. Kouzmekine, P. Iaizzo, J. Herzog, H. Lerche, S. Nicole, J. Vale-Santos, D. Chauveau, B. Fontaine, and F. Lehmann-Horn. 2000. Voltage-sensor sodium channel mutations cause hypokalemic periodic paralysis type 2 by enhanced inactivation and reduced current. *Proc. Natl. Acad. Sci. USA.* 97:9549–9554.

Kearney, J. A., N. W. Plummer, M. R. Smith, J. Kapur, T. R. Cummins, S. G. Waxman, A. L. Goldin, and M. H. Meisler. 2001. A gain-of-function mutation in the sodium channel gene Scn2a results in seizures and behavioral abnormalities. *Neuroscience.* 102:307–317.

Lerche, H., K. Jurkat-Rott, and F. Lehmann-Horn. 2001a. Ion channels and epilepsy. *Am. J. Med. Genet.* 106:146–159.

Lerche, H., Y. G. Weber, H. Baier, K. Jurkat-Rott, O. K. de Camargo, A. C. Ludolph, H. Bode, and F. Lehmann-Horn. 2001b. Generalized epilepsy with febrile seizures plus: further heterogeneity in a large family. *Neurology.* 57:1191–1198.

Lossin, C., T. H. Rhodes, R. R. Desai, C. G. Vanoye, D. Wang, S. Carniciu, O. Devinsky, and A. L. George, Jr. 2003. Epilepsy-associated dysfunction in the voltage-gated neuronal sodium channel SCN1A. *J. Neurosci.* 23:11289–11295.

Lossin, C., D. W. Wang, T. H. Rhodes, C. G. Vanoye, and A. L. George. 2002. Molecular basis of an inherited epilepsy. *Neuron.* 34:877–884.

Luo, C. H., and Y. Rudy. 1991. A model of the ventricular cardiac action potential. Depolarization, repolarization, and their interaction. *Circ. Res.* 68:1501–1526.

Luo, C. H., and Y. Rudy. 1994. A dynamic model of the cardiac ventricular action potential. I. Simulations of ionic currents and concentration changes. *Circ. Res.* 74:1071–1096.

MacDonald, B. T., A. Escayg, J. Spampanato, E. Montalenti, P. Benna, A. L. Goldin, and M. H. Meisler. 2001. A novel mutation of the sodium channel SCN1A in the epilepsy syndrome GEFS plus. *Am. J. Hum. Genet.* 69:600–600.

Maier, S. K. G., R. E. Westenbroek, W. A. Catterall, and T. Scheuer. 2003. TTX-sensitive brain-type sodium channels in the mouse SA node are required for regular sinus rhythm. *Biophys. J.* 84:421a–421a.

Maier, S. K. G., R. E. Westenbroek, K. A. Schenkman, E. O. Feigl, T. Scheuer, and W. A. Catterall. 2002. An unexpected role for brain-type sodium channels in coupling of cell surface depolarization to contraction in the heart. *Proc. Natl. Acad. Sci. USA.* 99:4073–4078.

McPhee, J. C., D. S. Ragsdale, T. Scheuer, and W. A. Catterall. 1995. Critical role for transmembrane segment IVS6 of the sodium-channel alpha-subunit in fast inactivation. *J. Biol. Chem.* 270:12025–12034.

Meisler, M. H., J. Kearney, A. Escayg, B. T. MacDonald, and L. K. Sprunger. 2001. Sodium channels and neurological disease: Insights from Scn8a mutations in the mouse. *Neuroscientist.* 7:136–145.

Meisler, M. H., J. A. Kearney, L. K. Sprunger, B. T. MacDonald, D. A. Buchner, and A. Escayg. 2002. Mutations of voltage-gated sodium channels in movement disorders and epilepsy. *Sodium Channels and Neuronal Hyperexcitability.* 241:72–86.

Migliore, M., E. P. Cook, D. B. Jaffe, D. A. Turner, and D. Johnston. 1995. Computer simulations of morphologically reconstructed CA3 hippocampal neurons. *J. Neurophysiol.* 73:1157–1168.

Noble, D. 2002a. The rise of computational biology. *Nat. Rev. Mol. Cell Biol.* 3:459–463.

Noble, D. 2002b. Unraveling the genetics and mechanisms of cardiac arrhythmia. *Proc. Natl. Acad. Sci. USA.* 99:5755–5756.

Nuyens, D., M. Stengl, S. Dugarmaa, T. Rossenbacker, V. Compernolle, Y. Rudy, J. F. Smits, W. Flameng, C. E. Clancy, L. Moons, M. A. Voss, M. Dewerchin, K. Benndorf, D. Collen, E. Carmeliet, and P. Carmeliet. 2001. Abrupt rate accelerations or premature beats cause life-threatening arrhythmias in mice with long-QT3 syndrome. *Nat. Med.* 7:1021–1027.

Spampanato, J., A. Escayg, M. H. Meisler, and A. L. Goldin. 2001. Functional effects of two voltage-gated sodium channel mutations that cause generalized epilepsy with febrile seizures plus type 2. *J. Neurosci.* 21:7481–7490.

Splawski, I., K. W. Timothy, M. Tateyama, C. E. Clancy, A. Malhotra, A. H. Beggs, F. P. Cappuccio, G. A. Sagnella, R. S. Kass, and M. T. Keating. 2002. Variant of SCN5A sodium channel implicated in risk of cardiac arrhythmia. *Science.* 297:1333–1336.

Steinlein, O. K. 2001. Genes and mutations in idiopathic epilepsy. *Am. J. Med. Genet.* 106:139–145.

Traub, R. D., J. G. R. Jefferys, R. Miles, M. A. Whittington, and K. Toth. 1994. A branching dendritic model of a rodent CA3 pyramidal neuron. *J. Physiol.* 481:79–95.

Traub, R. D., R. K. S. Wong, R. Miles, and H. Michelson. 1991. A model of a CA3 hippocampal pyramidal neuron incorporating voltage-clamp data on intrinsic conductances. *J. Neurophysiol.* 66:635–650.

Vandenberg, C. A., and R. Horn. 1984. Inactivation viewed through single sodium-channels. *J. Gen. Physiol.* 84:535–564.

Vanoye, C. G., C. Lossin, and A. L. George. 2003. Single-channel analysis of the human sodium channel SCN1A. *Biophys. J.* 84:68a–68a. (Abstr.)

Wehrens, X. H. T., H. Abriel, C. Cabo, J. Benhorin, and R. S. Kass. 2000. Arrhythmogenic mechanism of an LQT-3 mutation of the human heart Na^+ channel alpha-subunit: a computational analysis. *Circulation.* 102:584–590.

Weiss, L. A., A. Escayg, J. A. Kearney, M. Trudeau, B. T. MacDonald, M. Mori, J. Reichert, J. D. Buxbaum, and M. H. Meisler. 2003. Sodium channels SCN1A, SCN2A and SCN3A in familial autism. *Mol. Psychiatry.* 8:186–194.

Westenbroek, R. E., D. K. Merrick, and W. A. Catterall. 1989. Differential subcellular-localization of the Ri and Rii Na^+ channel subtypes in central neurons. *Neuron.* 3:695–704.